

Honest calibration assessment for binary outcome predictions

Timo Dimitriadis¹, Lutz Dümbgen², Alexander Henzi³, Marius Puke⁴, and Johanna Ziegel²

¹Heidelberg University, Germany

²University of Bern, Switzerland

³ETH Zürich, Switzerland

⁴University of Hohenheim, Germany

timo.dimitriadis@awi.uni-heidelberg.de, lutz.duembgen@stat.unibe.ch,
alexander.henzi@stat.math.ethz.ch, marius.puke@uni-hohenheim.de,
johanna.ziegel@stat.unibe.ch

November 4, 2022

Abstract

Probability predictions from binary regressions or machine learning methods ought to be calibrated: If an event is predicted to occur with probability x , it should materialize with approximately that frequency, which means that the so-called calibration curve $p(\cdot)$ should equal the identity, $p(x) = x$ for all x in the unit interval. We propose honest calibration assessment based on novel confidence bands for the calibration curve, which are valid only subject to the natural assumption of isotonicity. Besides testing the classical goodness-of-fit null hypothesis of perfect calibration, our bands facilitate inverted goodness-of-fit tests whose rejection allows for the sought-after conclusion of a sufficiently well specified model. We show that our bands have a finite sample coverage guarantee, are narrower than existing approaches, and adapt to the local smoothness of the calibration curve p and the local variance of the binary observations. In an application to model predictions of an infant having a low birth weight, the bounds give informative insights on model calibration.

Keywords: Binary regression, calibration validation, isotonic regression, confidence band, goodness-of-fit, universally valid inference

1 Introduction

Consider first a univariate regression setting with fixed real covariates $x_1 \leq \dots \leq x_n$ and independent binary observations $Y_1, \dots, Y_n \in \{0, 1\}$, where $\text{pr}(Y_i = 1) = p(x_i)$ for some unknown regression function $p : \mathbb{R} \rightarrow [0, 1]$. Standard parametric models for this setting, e.g. logistic or probit regression, involve monotone regression functions p . Thus, an interesting nonparametric alternative would be to draw inference on p under the sole assumption that it is isotonic on \mathbb{R} ,

$$p(x) \leq p(x'), \quad x \leq x'. \quad (1)$$

In the specific applications we have in mind, the x_i are themselves probability predictions for the binary outcomes, i.e. $x_i \in [0, 1]$ is a prediction for the probability of the event $\{Y_i = 1\}$. In practice, the predictions can be obtained from a test sample of binary regressions, machine learning methods, or any other statistical model for binary data. A reliable interpretation of these predictions relies on the property of calibration, meaning that if the value x_i is predicted,

the corresponding event should indeed occur with probability x_i . In this setting, the regression function p is called calibration curve, and it maps the predicted probabilities x_i to the actual, or recalibrated, event probabilities $p(x_i) = \text{pr}(Y_i = 1)$. For calibrated predictions, the calibration curve equals the diagonal, $p(x) = x$ for all $x \in [0, 1]$. Drawing inference about p thus allows to assess the calibration of the predictions.

Testing the null hypothesis of calibration, $\mathbb{H}_0: p(x) = x$ for all $x \in [0, 1]$, is closely related to goodness-of-fit testing, which is crucial in applications, see e.g., [Tutz \(2011, Section 4.2\)](#) and [Hosmer et al. \(2013, Chapter 5\)](#). It is still regularly carried out by the classical test of [Hosmer and Lemeshow \(1980\)](#), which groups the predictions x_i into bins and applies a χ^2 -test. It is however subject to multiple criticisms: First, its ad hoc choice of bins can result in untenable instabilities ([Bertolini et al., 2000](#); [Allison, 2014](#)). Second, placing the hypothesis of calibration in the null only allows for rejecting calibration rather than showing that a model is sufficiently well calibrated, where the latter would be highly desirable for applied researchers. Third, the test rejects essentially all, even acceptably well-specified models in large samples ([Nattino et al., 2020a](#); [Paul et al., 2013](#)), resulting in calls for a goodness-of-fit tests with inverted hypotheses ([Nattino et al., 2020b](#)), that is, tests where the hypothesis $p(x) = x$ is contained in the alternative.

We propose a statistically sound solution to these criticisms by constructing honest, simultaneous confidence bands (L^α, U^α) for the function p . That is, for a given small number $\alpha \in (0, 1)$ and $\mathcal{Y} := (Y_i)_{i=1}^n$, we compute data-dependent functions $L^\alpha = L^\alpha(\cdot, \mathcal{Y})$ and $U^\alpha = U^\alpha(\cdot, \mathcal{Y})$ on \mathbb{R} such that

$$\text{pr}\{L^\alpha \leq p \leq U^\alpha \text{ on } \mathbb{R}\} \geq 1 - \alpha. \quad (2)$$

In the context of calibration assessment, the functions p, L^α, U^α are defined on $[0, 1]$, and we call (L^α, U^α) a calibration band, which is hence a confidence band for the calibration curve. It allows for the desirable conclusion that with confidence $1 - \alpha$, the true calibration curve p lies inside the band, simultaneously for all values of the predicted probabilities. This nests a classical goodness-of-fit test with $\mathbb{H}_0: p(x) = x$ by checking whether the band contains the diagonal $d(x) = x$ for all relevant values $x \in [0, 1]$, but also any other hypothesis on the calibration curve such as e.g., an inverted goodness-of-fit test with $\mathbb{H}_0: |p(x) - x| > \epsilon$ for some small $\epsilon > 0$. Hence, this band resolves the above mentioned criticisms of classical goodness-of-fit tests.

Figure 1 shows the bands in a large data example for probit model predictions for the binary outcome of a fetus having a low birth weight. See Section 6 for additional details. The test of Hosmer and Lemeshow clearly rejects calibration even though our bands indicate a well-calibrated model by including the diagonal line for all values in the unit interval. The magnified right panel of the figure shows that with confidence $1 - \alpha$, the model is remarkably well calibrated for the most important region of small probability predictions in this application. It is important to notice that even though we build our bands on the model predictions, the methodology applies equally to both, causal and predictive regressions. An open-source implementation in the statistical software R ([R Core Team, 2022](#)) is available under <https://cran.r-project.org/package=calibrationband>.

Our confidence bands are valid in finite samples subject only to the mild monotonicity assumption at (1), implying that higher predictions entail a higher probability for $\{Y = 1\}$, which is natural in the context of assessing calibration as already argued in [Dimitriadis et al. \(2021\)](#); [Roelofs et al. \(2020\)](#). For classical goodness-of-fit tests, the null hypothesis $p(x) = x$ already nests the monotonicity assumption and if a researcher aims to demonstrate calibration, i.e., $p(x) = x$ holds at least approximately, it is unlikely that there are strong deviations from isotonicity. Moreover, our confidence bands allow to detect and quantify violations of monotonicity as described in Appendix A. A non-monotonic p may lead to a crossing of the lower and upper bound, i.e., $U^\alpha(x) < L^\alpha(x)$ for some x , which allows to reject monotonicity at level α . This is supported by the graphical display that reacts to non-isotonicity by generating elongated horizontal segments in both, the isotonic regression estimate and the confidence bands. Finally,

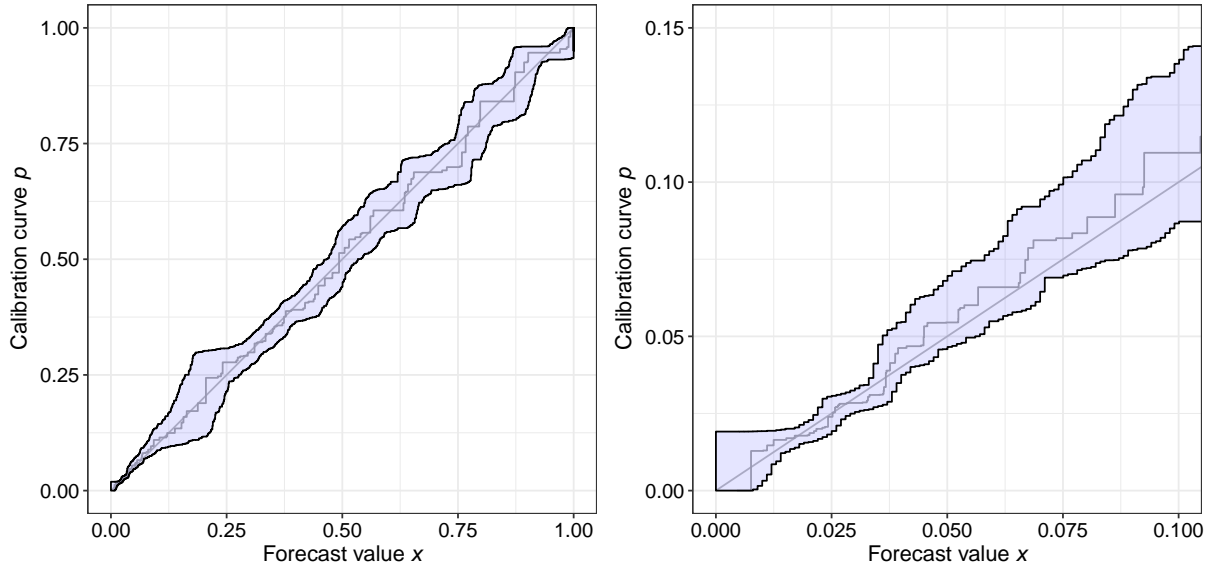


Figure 1: Left: Confidence band for the calibration curve (denoted calibration band in the application section) for the first model specification of the low birth weight application in Section 6. The blue band shows the confidence band based on the non-crossing method in (6) together with the rounding in (7) with $K = 10^3$, and the grey step function shows the isotonic regression estimate. Right: Magnified version focusing on predicted probabilities below 10%.

deriving confidence bands without any assumption on p seems unrealistic and the assumption of monotonicity is relatively weak, e.g., in comparison to the parametric one used in [Nattino et al. \(2014\)](#).

As expected for a non-parametric, pathwise and almost universally valid confidence band, we require large data sets of at least 5000 observations to obtain sensibly narrow bands. These are exactly the sample sizes where the classical goodness-of-fit tests become uninformative by rejecting all models in applications, see the simulation study of [Kramer and Zimmerman \(2007\)](#).

A theoretical analysis shows that the proposed confidence band adapts locally to the smoothness of the function p and to the variance of the observations. Adaptivity to the smoothness means that the width of the bands decreases faster with the sample size n in regions where p is constant, and at a slower rate where p is steeper. This property is known for more general confidence bands for a monotone mean function developed by [Yang and Barber \(2019\)](#). Adaptivity to the variance means that the band is substantially narrower at x if $p(x)$ is close to zero or one, compared to $p(x)$ near 0.5. In many practical applications, including the low birth weight predictions analyzed in this article, predicted probabilities close to zero or one are of most relevance and a sharp assessment of calibration in these regions is particularly important.

Existing methods for the construction of confidence bands in this setting are rare with the following two exceptions: First, [Nattino et al. \(2014\)](#) propose the use of confidence bands based on a parametric assumption on the function p , which we show to have incorrect coverage in almost all of our simulation settings. Second, the nonparametric bands of [Yang and Barber \(2019\)](#) are valid, in a modified sense even in settings where the isotonicity assumption (1) is violated. But they are shown to be wider than our bands in theory and simulations.

We explain the absence of competing methods by their theoretical difficulties. Using asymptotic theory of the isotonic regression estimator is complicated as it requires the estimation of nuisance quantities such as the derivative of the unknown function p , the convergence rate depends on the functional form of p , it is subject to more restrictive assumptions and only results in bands with a pointwise interpretation ([Wright, 1981](#)). Resampling schemes are theoretically found to be inconsistent for the isotonic regression ([Sen et al., 2010](#); [Guntuboyina and Sen,](#)

2018). Other non-parametric approaches in the literature for constructing confidence bands for functions, many of them presented in the review by [Hall and Horowitz \(2013\)](#), are often pointwise, not simultaneous, and require the selection of tuning parameters that may lead to instabilities, similar to the choice of the bins in the Hosmer-Lemeshow test. In contrast, the confidence bands proposed here are simple to compute and do not involve any implementation decisions resulting in a stable and reproducible method as called for by [Stodden et al. \(2016\)](#); [Yu and Kumbier \(2020\)](#).

2 Construction of the confidence bands

Within the regression setting, we construct confidence bands for the isotonic regression function p by means of the classical confidence bounds of [Clopper and Pearson \(1934\)](#) for a binomial parameter. Suppose that Z is a binomial random variable with parameters m and $q \in [0, 1]$. For $\delta \in (0, 1)$ let

$$\begin{aligned} u^\delta(Z, m) &= \max\{\xi \in [0, 1]: \text{pbin}(Z, m, \xi) \geq \delta\} \\ &= \begin{cases} \text{qbeta}(1 - \delta, Z + 1, m - Z), & Z < m, \\ 1, & Z = m, \end{cases} \\ \ell^\delta(Z, m) &= \min\{\xi \in [0, 1]: \text{pbin}(Z - 1, m, \xi) \leq 1 - \delta\} \\ &= \begin{cases} \text{qbeta}(\delta, Z, m + 1 - Z), & Z > 0, \\ 0, & Z = 0. \end{cases} \end{aligned}$$

Here $\text{pbin}(\cdot, m, \xi)$ denotes the distribution function of the binomial distribution with parameters m and ξ , while $\text{qbeta}(\cdot, a, b)$ stands for the quantile function of the beta distribution with parameters $a, b > 0$. Then

$$\text{pr}\{q \leq u^\delta(Z, m)\} \geq 1 - \delta \quad \text{and} \quad \text{pr}\{q \geq \ell^\delta(Z, m)\} \geq 1 - \delta.$$

For the representation of $\ell^\delta(Z, m)$ and $u^\delta(Z, m)$ in terms of beta quantiles, we refer to [Johnson et al. \(2005\)](#).

Assumption (1) allows to construct confidence bands for p as follows. With $p_i := p(x_i)$, for arbitrary indices $1 \leq j \leq k \leq n$, the random sum

$$Z_{jk} = \sum_{i=j}^k Y_i$$

is stochastically larger than a binomial random variable with parameters $n_{jk} = k - j + 1$ and p_j , and it is stochastically smaller than a binomial variable with parameters n_{jk} and p_k . Thus, as explained in Lemma B1,

$$\text{pr}\{p_j \leq u^\delta(Z_{jk}, n_{jk})\} \geq 1 - \delta, \quad \text{pr}\{p_k \geq \ell^\delta(Z_{jk}, n_{jk})\} \geq 1 - \delta. \quad (3)$$

If we combine these bounds for all pairs (j, k) in a given set \mathcal{J} and use the assumption at (1), then we may claim with confidence $1 - 2|\mathcal{J}|\delta$ that simultaneously for all $(j, k) \in \mathcal{J}$,

$$p(x) \leq u^\delta(Z_{jk}, n_{jk}) \quad \forall x \leq x_j, \quad p(x) \geq \ell^\delta(Z_{jk}, n_{jk}) \quad \forall x \geq x_k.$$

Specifically, let \mathcal{J} be the set of all index pairs (j, k) such that $j \leq k$ and $x_{j-1} < x_j$ and $x_k < x_{k+1}$. If there are tied values in $(x_i)_{i=1}^n$, \mathcal{J} selects the outermost indices of the tied values. Hence, if $\{x_1, \dots, x_n\}$ contains $N \leq n$ different points, then $|\mathcal{J}| = (N^2 + N)/2$. Consequently, for a given confidence level $1 - \alpha \in (0, 1)$, we may combine the bounds $u^\delta(Z_{jk}, n_{jk})$ and $\ell^\delta(Z_{jk}, n_{jk})$ with $\delta = \alpha/(N^2 + N)$ to obtain a first confidence band.

Theorem 1. For $x \in \mathbb{R}$, let

$$U^{\alpha, \text{raw}}(x) = \inf_{(j,k) \in \mathcal{J}: x_j \geq x} u^{\alpha/(N^2+N)}(Z_{jk}, n_{jk}), \quad (4)$$

$$L^{\alpha, \text{raw}}(x) = \sup_{(j,k) \in \mathcal{J}: x_k \leq x} \ell^{\alpha/(N^2+N)}(Z_{jk}, n_{jk}), \quad (5)$$

where $\inf_{\emptyset} := 1$ and $\sup_{\emptyset} := 0$. If p satisfies the isotonicity assumption at (1), then the resulting confidence band $(L^{\alpha, \text{raw}}, U^{\alpha, \text{raw}})$ satisfies requirement (2).

The functions $U^{\alpha, \text{raw}}, L^{\alpha, \text{raw}}$ are isotonic and piecewise constant. Precisely, with $x_0 := -\infty$ and $x_{n+1} := \infty$, we know that $U^{\alpha, \text{raw}} = 1$ on (x_n, ∞) , $L^{\alpha, \text{raw}} = 0$ on $(-\infty, x_1)$, and

$$\begin{aligned} U^{\alpha, \text{raw}}(x) &= U^{\alpha, \text{raw}}(x_i), & x \in (x_{i-1}, x_i], \\ L^{\alpha, \text{raw}}(x) &= L^{\alpha, \text{raw}}(x_i), & x \in [x_i, x_{i+1}), \end{aligned}$$

for $i = 1, \dots, n$. Consequently, computing the band $(L^{\alpha, \text{raw}}, U^{\alpha, \text{raw}})$ amounts to determining the $2n$ numbers $L^{\alpha, \text{raw}}(x_i)$ and $U^{\alpha, \text{raw}}(x_i)$, $i = 1, \dots, n$.

The confidence band proposed in Theorem 1 has two potential drawbacks. First, a natural nonparametric estimator for the function p under the assumption (1) is given by a minimizer \hat{p} of $\sum_{i=1}^n \{h(x_i) - Y_i\}^2$ over all isotonic functions $h: [0, 1] \rightarrow [0, 1]$ (Dimitriadis et al., 2021). This minimizer is unique on the set $\{x_1, \dots, x_n\}$. But there is no guarantee that $L^{\alpha, \text{raw}} \leq \hat{p} \leq U^{\alpha, \text{raw}}$. Second, the upper and lower bounds in (4) and (5) may even cross, resulting in an empty, and hence, nonsensical confidence band. These problems can be dealt with by using the non-crossing confidence band $(L^{\alpha, \text{nc}}, U^{\alpha, \text{nc}})$ given by pointwise minima and maxima:

$$L^{\alpha, \text{nc}} = \min(L^{\alpha, \text{raw}}, \hat{p}), \quad U^{\alpha, \text{nc}} = \max(L^{\alpha, \text{raw}}, \hat{p}). \quad (6)$$

Obviously, $L^{\alpha, \text{nc}} \leq \hat{p} \leq U^{\alpha, \text{nc}}$ on \mathbb{R} . Our simulation experiments indicate that $(L^{\alpha, \text{raw}}, U^{\alpha, \text{raw}}) = (L^{\alpha, \text{nc}}, U^{\alpha, \text{nc}})$ holds in almost all cases whenever p satisfies (1); see Section 5 for details. The potential crossing of the two bounds in Theorem 1 also has an advantage. It allows for inference about the non-isotonicity of p , see Appendix A.

A potential obstacle in the practical application of the confidence bands proposed in this section is that their computation requires $\mathcal{O}(N^2)$ steps. This can be relieved by using a smaller family of index pairs (j, k) in the definition of the confidence band. Specifically, if for some fixed integer $K \geq 1$ differences in the covariate smaller than K^{-1} are regarded as negligible, then one could define

$$\tilde{\mathcal{J}} = \{(j, k): \{x_j, \dots, x_k\} = \{x_1, \dots, x_n\} \cap [r/K, s/K] \text{ for some } r, s \in \mathbb{Z}\}, \quad (7)$$

such that only blocks of covariate values between r/K and s/K , $r, s \in \mathbb{Z}$, are considered. The resulting band is still honest, can be computed in $\mathcal{O}(|\tilde{\mathcal{J}}|)$ steps, and one can reduce the correction factor of the significance level in (4) and (5) from $N^2 + N$ to $|\tilde{\mathcal{J}}|$. The drawback is that the constant regions in L^α and U^α become larger, thereby limiting the adaptivity of the band, so the number K should not be too small. We henceforth refer to the restricted choice of $\tilde{\mathcal{J}}$ in (7) as the rounding method. Section 1 in the Supplementary Material illustrates in simulations that the rounding method drastically decreases the computation time and even results in narrower bands for all but very steep regions of p .

3 Relation to Yang and Barber (2019)

The methods of Yang and Barber (2019) may be adapted to the present regression setting with covariates $x_1 \leq \dots \leq x_n$ as follows: With the isotonic estimator \hat{p} introduced before, let

$$Z_{jk}^{\text{iso}} = \sum_{i=j}^k \hat{p}(x_i).$$

Set

$$U^{\alpha, \text{YB}}(x) = \inf_{(j,k) \in \mathcal{J}: x_j \geq x} \left[\frac{Z_{jk}^{\text{iso}}}{n_{jk}} + \sqrt{\frac{\log\{(N^2 + N)/\alpha\}}{2n_{jk}}} \right], \quad (8)$$

$$L^{\alpha, \text{YB}}(x) = \sup_{(j,k) \in \mathcal{J}: x_k \leq x} \left[\frac{Z_{jk}^{\text{iso}}}{n_{jk}} - \sqrt{\frac{\log\{(N^2 + N)/\alpha\}}{2n_{jk}}} \right]. \quad (9)$$

This defines a confidence band $(L^{\alpha, \text{YB}}, U^{\alpha, \text{YB}})$ with the following property:

$$\text{pr}\{L^{\alpha, \text{YB}} \leq \tilde{p} \leq U^{\alpha, \text{YB}} \text{ on } \mathbb{R}\} \geq 1 - \alpha, \quad (10)$$

where $\tilde{p}: \mathbb{R} \rightarrow [0, 1]$ is any fixed isotonic function minimizing $\sum_{i=1}^n \{\tilde{p}(x_i) - p_i\}^2$. Thus one obtains a confidence band with guaranteed coverage probability $1 - \alpha$ for an isotonic approximation of p , even if (1) is violated. The proof of (10) follows from the arguments of Yang and Barber (2019), noting that the random variables Y_i are sub-Gaussian with scale parameter $\sigma = 1/2$. Thus, $\mathbb{E} \exp(t(Y_i - p_i)) \leq \exp(\sigma^2 t^2 / 2)$ for all $t \in \mathbb{R}$, implying that for arbitrary $\eta \geq 0$,

$$\text{pr}\{\pm(Z_{jk} - \mathbb{E}Z_{jk}) \geq \eta\} \leq \exp(-2n_{jk}\eta^2),$$

see Hoeffding (1963). The following result shows that the confidence bands $(L^{\alpha, \text{raw}}, U^{\alpha, \text{raw}})$ and $(L^{\alpha, \text{nc}}, U^{\alpha, \text{nc}})$ are always contained in the band $(L^{\alpha, \text{YB}}, U^{\alpha, \text{YB}})$.

Theorem 2. For all $\alpha \in (0, 1)$ and any data vector $\mathcal{Y} \in \{0, 1\}^n$,

$$L^{\alpha, \text{YB}} \leq L^{\alpha, \text{nc}} \leq L^{\alpha, \text{raw}}, \quad U^{\alpha, \text{raw}} \leq U^{\alpha, \text{nc}} \leq U^{\alpha, \text{YB}} \text{ on } \mathbb{R}.$$

Recall that the inequalities $L^{\alpha, \text{raw}} \leq U^{\alpha, \text{raw}}$ do not hold in general, and a crossing of the bounds allows to reject isotonicity at level α , see Appendix A. In contrast, the bands by Yang and Barber (2019) always contain the isotonic estimator \hat{p} , and are guaranteed to cover an optimal isotonic approximation of p with probability at least $1 - \alpha$. For calibration testing, the possibility of rejecting isotonicity seems more desirable than information about an isotonic approximation of the calibration curve, whose interpretation may be unclear in practice. It should be mentioned, however, that the band $(L^{\alpha, \text{YB}}, U^{\alpha, \text{YB}})$ has a computational advantage. For the computation of $U_i^{\alpha, \text{YB}}$ in (8), it suffices to take the minimum over endpoints of constancy regions of \hat{p} , that is, all $(j, k) \in \mathcal{J}$ such that $j = \min\{s: x_s \geq x_i\}$ and $\hat{p}(x_k) < \hat{p}(x_{k+1})$ or $k = n$, see Proposition B1. Likewise, for the computation of $L_i^{\alpha, \text{YB}}$ in (9), it suffices to take the maximum over all $(j, k) \in \mathcal{J}$ such that $\hat{p}(x_{j-1}) < \hat{p}(x_j)$ or $j = 1$ and $k = \max\{s: x_s \leq x_i\}$. While the computation of $(L^{\alpha, \text{raw}}, U^{\alpha, \text{raw}})$ or $(L^{\alpha, \text{nc}}, U^{\alpha, \text{nc}})$ requires $\mathcal{O}(N^2)$ steps, the following lemma, whose proof is in the Supplementary Material, implies that the computation of $(L^{\alpha, \text{YB}}, U^{\alpha, \text{YB}})$ requires only $\mathcal{O}(N \min\{n^{2/3}, N\})$ steps.

Lemma 1. The cardinality of $\{\hat{p}(x_i): i = 1, \dots, n\}$ is smaller than $3n^{2/3}$.

4 Theoretical properties of the confidence bands

This section illustrates consistency and adaptivity properties of the confidence band $(L_n^{\alpha, \text{raw}}, U_n^{\alpha, \text{raw}})$, where the subscript n indicates the sample size, and we consider a triangular scheme of observations $(x_i, Y_i) = (x_{ni}, Y_{ni})$, $i = 1, \dots, n$. We are interested in situations in which the observed covariates x_{ni} could be the realizations of the order statistics of a random sample. Thus we extend the framework of Yang and Barber (2019) and consider the following assumption.

Assumption 1. Let $\text{Leb}(\cdot)$ denote Lebesgue measure, and let $W_n(B) = \#\{i: x_{ni} \in B\}$ for $B \subset \mathbb{R}$. There exist a non-degenerate interval $[a_o, b_o]$ and constants $C_1, C_2 > 0$ such that for sufficiently large n ,

$$W_n(B) \geq C_1 n \text{Leb}(B)$$

for arbitrary intervals $B \subset [a_o, b_o]$ such that $\text{Leb}(B) \geq C_2 \log(n)/n$.

This assumption comprises the setting of [Yang and Barber \(2019\)](#). Let G be a differentiable distribution function on $[0, 1]$ such that G' is bounded away from 0 on $[a_o, b_o]$. If $x_{ni} = G^{-1}(i/n)$ for $i = 1, \dots, n$, then it is satisfied for any $C_1 < \inf_{[a_o, b_o]} G'$ and arbitrary $C_2 > 0$. The arguments in [Mösching and Dümbgen \(2020, Section 4.3\)](#) can be modified to show that if x_{n1}, \dots, x_{nn} are the order statistics of n independent random variables with distribution function G , then Assumption 1 is satisfied almost surely, provided that $C_1, C_2 > 0$ are chosen appropriately.

Theorem 3. *Suppose that Assumption 1 is satisfied. Let $\rho_n = \log(n)/n$. There exist constants $C > 0$ depending only on C_1, C_2 with the following properties:*

(i) *Suppose that p is constant on $[a_o, b_o]$. With asymptotic probability one,*

$$\begin{aligned} U_n^{\alpha, \text{raw}}(x) &\leq p(x) + C\sqrt{\rho_n/(b_o - x)}, & x \in [a_o, b_o), \\ L_n^{\alpha, \text{raw}}(x) &\geq p(x) - C\sqrt{\rho_n/(x - a_o)}, & x \in (a_o, b_o]. \end{aligned}$$

(ii) *Suppose that p is Lipschitz-continuous on $[a_o, b_o]$ with Lipschitz constant $L > 0$. With asymptotic probability one,*

$$\begin{aligned} U_n^{\alpha, \text{raw}}(x) &\leq p(x) + C(L\rho_n)^{1/3}, & x \in [a_o, b_o - \rho_n^{1/3}L^{-2/3}], \\ L_n^{\alpha, \text{raw}}(x) &\geq p(x) - C(L\rho_n)^{1/3}, & x \in [a_o + \rho_n^{1/3}L^{-2/3}, b_o]. \end{aligned}$$

(iii) *Suppose that p is discontinuous at some point $x_o \in (a_o, b_o)$. With asymptotic probability one,*

$$\begin{aligned} U_n^{\alpha, \text{raw}}(x) &\leq p(x_o-) + C\sqrt{\rho_n/(x_o - x)}, & x \in [a_o, x_o), \\ L_n^{\alpha, \text{raw}}(x) &\geq p(x_o+) - C\sqrt{\rho_n/(x - x_o)}, & x \in (x_o, b_o]. \end{aligned}$$

(iv) *Suppose that $\lim_{x \rightarrow a_o} p(x) = 0$. For sufficiently large n ,*

$$\mathbb{E}\{U_n^{\alpha, \text{raw}}(x)\} \leq C \inf_{y \in (x, b_o)} \{p(y) + \rho_n/(y - x)\}, \quad x \in [a_o, b_o].$$

Analogously, if $\lim_{x \rightarrow b_o} p(x) = 1$, then for sufficiently large n ,

$$\mathbb{E}\{1 - L_n^{\alpha, \text{raw}}(x)\} \leq C \inf_{y \in [a_o, x)} \{1 - p(y) + \rho_n/(x - y)\}, \quad x \in (a_o, b_o].$$

Part (i) implies that if p is constant on $[a_o, b_o]$, then for arbitrary fixed $a_o < a < b < b_o$,

$$\sup_{x \in [a_o, b]} \{U_n^{\alpha, \text{raw}}(x) - p(x)\}^+ + \sup_{x \in [a_o, b]} \{p(x) - L_n^{\alpha, \text{raw}}(x)\}^+ = \mathcal{O}_p(\rho_n^{1/2}).$$

Thus, parts (i-ii) of this theorem are analogous to results of [Yang and Barber \(2019, Sections 4.4 and 4.6\)](#). Part (iii) implies that with asymptotic probability one,

$$U_n^{\alpha, \text{raw}}(x) < \frac{p(x_o-) + p(x_o+)}{2} < L_n^{\alpha, \text{raw}}(y)$$

for $x < x_o - D\rho_n$, $y > x_o + D\rho_n$ and $D = 4C^2\{p(x_o+) - p(x_o-)\}^{-2}$. Thus, at points of discontinuity of p , the confidence band crosses a horizontal line on an interval of length $\mathcal{O}_p(\rho_n)$. Part (iv) demonstrates that our bounds are particularly accurate in regions where $p(x)$ is close to 0 or 1. Specifically, suppose that for some $\gamma > 0$, $p(x) = \mathcal{O}\{(x - a_o)^\gamma\}$ for $x \in [a_o, b_o]$. Then plugging in $y(x) = x + \rho_n^{1/(\gamma+1)}$ reveals that

$$\mathbb{E}\{U_n^{\alpha, \text{raw}}(x)\} \leq D\{(x - a_o)^\gamma + \rho_n^{\gamma/(\gamma+1)}\}, \quad x \in [a_o, b_o],$$

where $D = D(C_1, C_2, p)$. Analogously, if $1 - p(x) = \mathcal{O}\{(b_o - x)^\gamma\}$ for $x \in [a_o, b_o]$, then

$$\mathbb{E}\{1 - L_n^{\alpha, \text{raw}}(x)\} \leq D\{(b_o - x)^\gamma + \rho_n^{\gamma/(\gamma+1)}\}, \quad x \in [a_o, b_o].$$

Presumably, the conclusions in part (iv) are not satisfied for the confidence band $(L_n^{\alpha, \text{YB}}, U_n^{\alpha, \text{YB}})$.

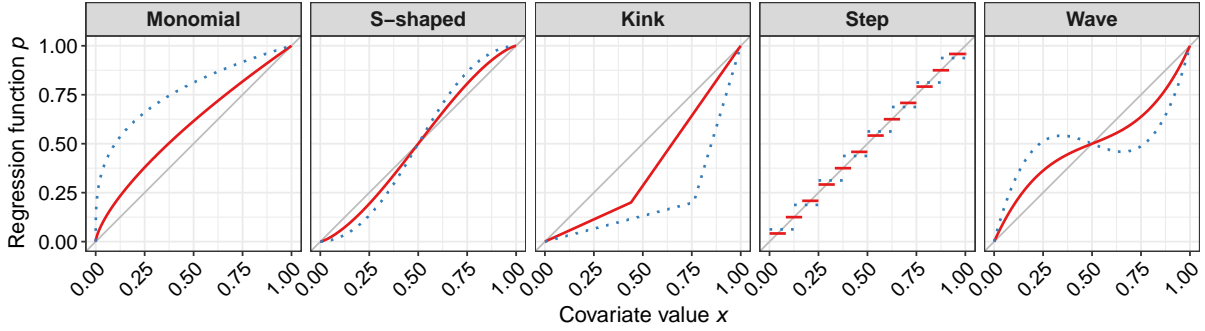


Figure 2: Illustration of the five simulated regression functions $p_s(\cdot)$, where the solid red line corresponds to the shape parameter value $s = 0.3$ and the dashed blue line to $s = 0.7$.

5 Simulations

Here, we illustrate that our confidence bands have correct coverage in the sense of (2) and are narrower than existing techniques. We consider both, the raw method in (4) and (5) and the non-crossing variant in (6). Both methods are combined with the rounding technique in (7) with $K = 10^3$ in order to facilitate faster computation at a minimal cost in accuracy. For comparison, we use the bands of Yang and Barber (2019) given in (8) and (9) with a minimal variance factor of $\sigma^2 = 1/4$ and the parametric bands of Nattino et al. (2014), implemented in the GivitiR package in the statistical software R (R Core Team, 2022). Replication material for the simulations and applications is available under https://github.com/marius-cp/replication_DDHPZ22.

We use 1000 replications, a significance level of $\alpha = 0.05$ and simulate the covariates $X \sim U[0, 1]$. The binary outcomes are generated by $Y \sim \text{Bern}\{p_s(X)\}$ based on five distinct functional forms of the regression function $p_s(x)$ for $x \in [0, 1]$ depending on a shape parameter $s \in \mathcal{S} := \{0, 0.1, \dots, 1\}$. The first four specifications of $p_s(x)$ satisfy the isotonicity assumption at (1) and cover smooth, non-smooth as well as discontinuous setups. The last one contains non-isotonic functions $p_s(x)$ for $s > 0.5$. The choice $s = 0$ results in the diagonal line $p_0(x) = x$ whereas the deviation from the diagonal increases with s . In particular, we consider the following specifications, which are illustrated in Figure 2 for two exemplary shape values $s \in \{0.3, 0.7\}$.

1. Monomial: First, we use the regression function $p_s(x) = x^{1-s}$, where $s \in \mathcal{S} \setminus \{1\}$. This function is already used in the simulations in Dimitriadis et al. (2021, Appendix A).
2. S-shaped: Second, the regression function follows an S-shaped form $p_s(x) = (1 + ((1-x)/x)^{1+s})^{-1}$, where $s \in \mathcal{S}$ pronounces the curves for larger values of s .
3. Kink: Third, $p_s(x)$ linearly interpolates the points $(0, 0)$, $(0.2 + 0.8s, 0.2)$ and $(1, 1)$ for $s \in \mathcal{S}$, resulting in a kink at the point $(0.2 + 0.8s, 0.2)$ for all $s > 0$.
4. Step: Fourth, we use a step function with $s^* \in \{5, 6, \dots, 14\}$ equidistant steps in the unit interval. It is given by $p_s(x) = \{\lfloor s^*x \rfloor + \mathbf{1}(x \neq 1)\} / s^*$, where $s^* = 15 - 10s$ and $s \in \mathcal{S} \setminus \{0\}$. It doesn't nest the diagonal, but the deviation from it increases with s .
5. Wave: Fifth, we use the cubic function $p_s(x) = 0.5 - (2s - 1)(x - 0.5) + 8s(x - 0.5)^3$ that violates the isotonicity assumption in (1) for any $s > 0.5$.

Figure 3 presents the average coverage rates for a range of sample sizes between 512 and 32 768. We use the raw method for our bands in (4) and (5) as the raw bands are contained in the non-crossing ones. We find that, as predicted by the theory, our confidence bands have conservative coverage throughout all isotonic simulation setups and sample sizes. We observe

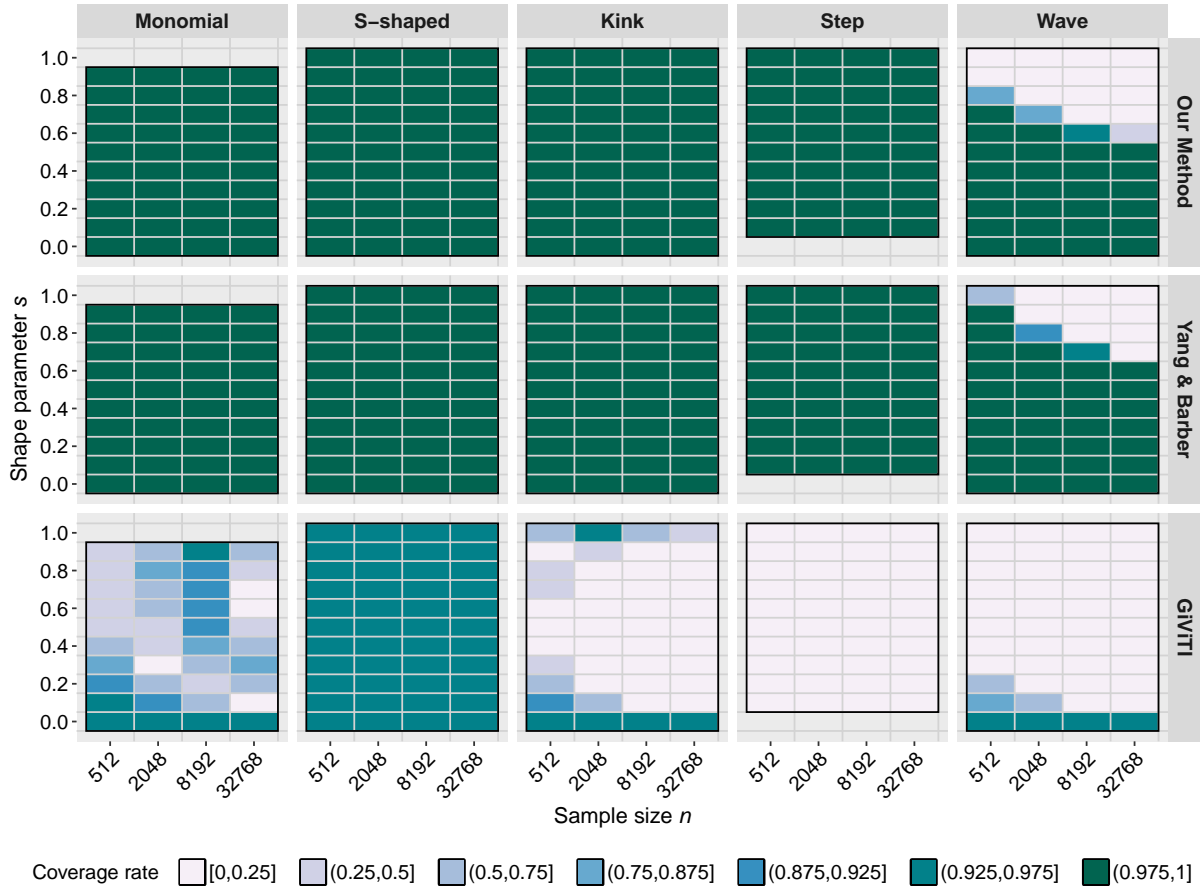


Figure 3: Empirical coverage rates of our confidence bands, the bands of [Yang and Barber \(2019\)](#), and the GiVITi bands for $1 - \alpha = 0.95$, averaged over all covariate values for the five specifications of the regression function $p_s(\cdot)$, different shape values s and a range of sample sizes n . For our bands, we use the raw method in (4) and (5), together with rounding in (7) with $K = 10^3$. The choices $s = 1$ in the Monomial, and $s = 0$ in Step specification are not defined.

coverage rates above 0.998 with the majority of 162 out of the 192 displayed coverage values being exactly one. The unreported non-crossing bands differ from the raw ones in less than one out of a hundred thousand instances. These deviations occur exclusively for large values of s in the Step specification within constancy regions of the function p . As expected, our method as well as the bands of [Yang and Barber \(2019\)](#) have incorrect coverage rates for the values $s > 0.5$ that violate isotonicity in the Wave specification when the sample size increases. The coverage rates of the [Yang and Barber \(2019\)](#) bands are still larger as these are shown to be wider by [Theorem 2](#).

The parametric bands of [Nattino et al. \(2014\)](#) rarely achieve correct coverage rates unless in the cases $s = 0$ and for the S-shaped regression functions. This can be explained as these bands are based on the assumption of a certain parametric form of $p_s(x)$, which is rarely satisfied. The results get worse for the non-smooth, the discontinuous and the non-isotonic specifications.

Figure 4 displays the average widths of our and the [Yang and Barber \(2019\)](#) bands. We present the theoretically wider non-crossing bands instead of the raw versions thereof. Their average widths is however non-distinguishable in these displays. We fix a medium degree of miscalibration $s = 0.5$. The upper plot panel displays the widths averaged over all simulation runs and values $x \in [0, 1]$ depending on the sample size n . We find that the size of both bands shrinks with n and that we can reconfirm the ordering established in [Theorem 2](#). We further see that our bands are only narrow enough for practical use in large samples. The relative gain in width of our bands is the highest for large sample sizes, exactly for which we propose the

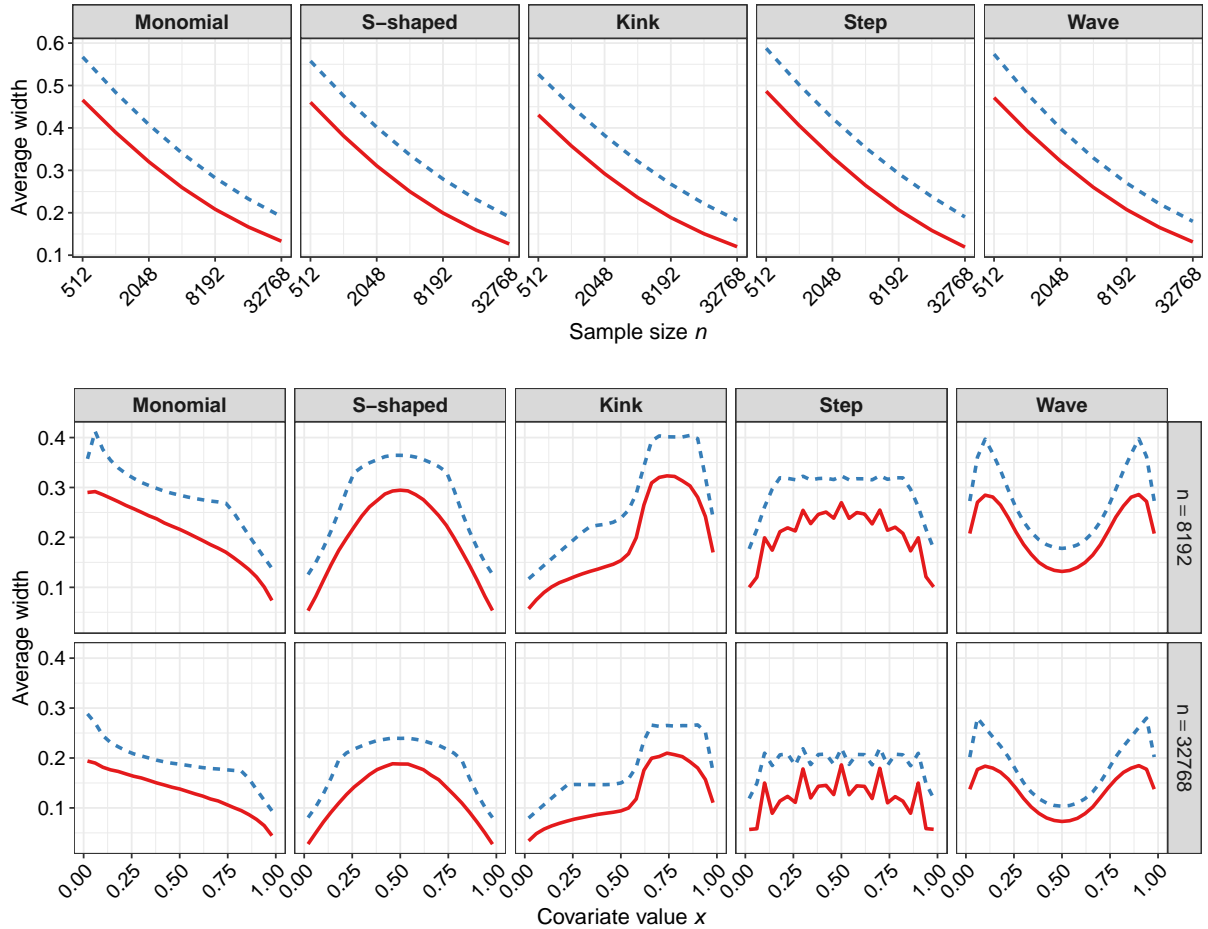


Figure 4: Top: Average widths of the 95% confidence bands by sample size for each of the five specifications of $p_s(x)$ given in the main text for a fixed value $s = 0.5$. Bottom: Average widths by covariate value x for two sample sizes. In both panels, the solid red line corresponds to our bands based on the non-crossing method in (6) together with rounding in (7) with $K = 10^3$, and the dashed blue line corresponds to the Yang and Barber (2019) bands.

application of our method for calibration validation. It is worth noting that the bands of Yang and Barber (2019) are more generally valid than for the special case of binary observations.

The lower plot panel shows the widths averaged over the simulation replications, but depending on the values $x \in [0, 1]$ for two selected sample sizes. It shows that the relative gains in width upon the bands of Yang and Barber (2019) are particularly pronounced close to the edges of the unit interval. In applications to calibration assessment, these regions of predicted probabilities close to zero or one are often of the highest interest as for example in the subsequent section assessing the goodness-of-fit of low birth weight probability predictions.

6 Application: Predicting low birth weight probabilities

We apply our confidence bands to assess calibration of three binary regression specifications predicting the probability of a fetus having a low birth weight, defined as weighting less than 2500 grams at birth (World Health Organization, 2015). Recall that in the setting of calibration assessment, we call the function p the calibration curve and our confidence bands are denoted as calibration bands. This follows the interpretation that for an event predicted with probability x , $p(x)$ denotes its true but unknown event probability. Perfectly calibrated predictions entail a calibration curve matching the diagonal line, $d(x) = x$. As the calibration band is a simulta-

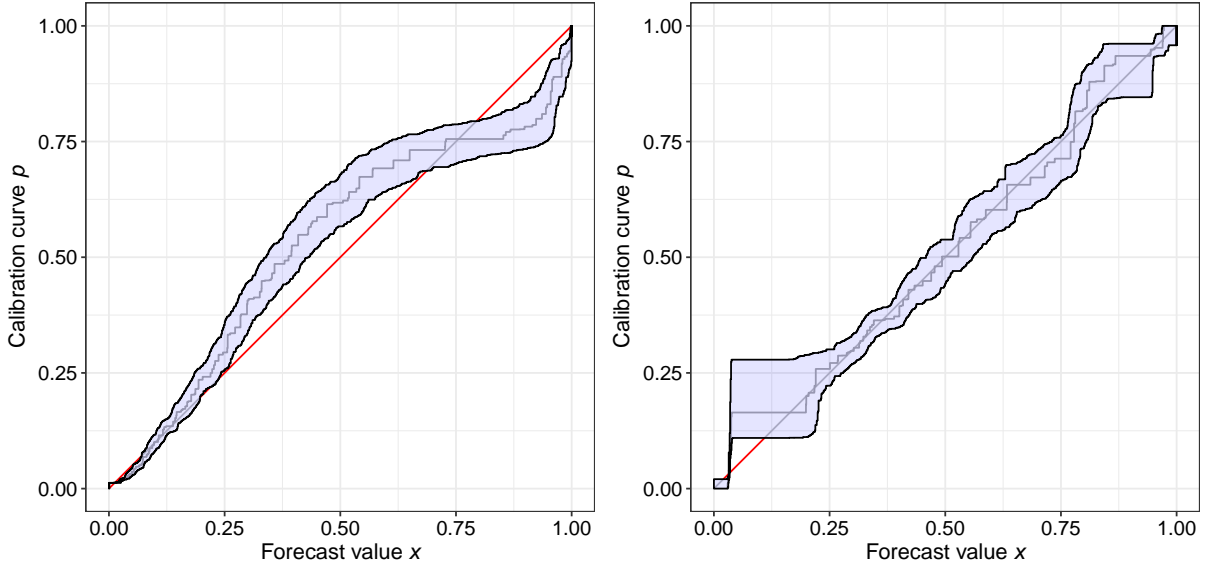


Figure 5: Calibration bands for the second model specification on the left and for the third specification on the right for the low birth weight application. The blue band denotes the calibration band based on the non-crossing method in (6) together with the rounding in (7) with $K = 10^3$, and the grey step function shows the isotonic regression estimate. The diagonal line is given in red color whenever it is not contained in the calibration band.

neously valid confidence band for p , deviations of the calibration band from the diagonal line imply significantly miscalibrated predictions in this region.

We use U.S. Natality Data from the [National Center for Health Statistics \(2017\)](#), which provides demographic and health data for 3 864 754 births in the year 2017. For the data set at hand, a low birth weight is observed in 8.1% of the cases. We estimate three binary regression models by maximum likelihood on the same randomly drawn subset that contains all but 1 000 000 observations that we leave for external model validation. All three models contain standard risk factors such as the mother’s age, body mass index and smoking behavior but they differ as follows. The first model uses a probit link function, and the explanatory variable week of gestation is categorized into four left-closed and right-open intervals with lower interval limits of 0, 28, 32 and 37 weeks, pertaining to the standard definitions of the World Health Organization of extremely, very, moderate and non preterm ([Quinn et al., 2016](#)). Through this categorization, the model specification can capture the week of gestation in a non-linear fashion. In contrast, the second model uses the week of gestation as a continuous explanatory variable and the third specification employs the cauchit instead of the probit link function, which is known to produce less confident predictions close to zero and one ([Koenker and Yoon, 2009](#)). Additional details of the model specifications are given in the Supplementary Material.

The classical Hosmer-Lemeshow test rejects perfect calibration of all three models with p-values of essentially zero for both, internal and external model validation, which leaves an applied researcher without any useful conclusions on model calibration. We show our calibration bands based on the non-crossing method with rounding to three digits, i.e., $K = 10^3$ in (7), with a confidence level of $1 - \alpha = 95\%$ for the first model in Figure 1 and for the other two models in Figure 5. We constantly extrapolate the bands on the unit interval which preserves their theoretical coverage guarantees as discussed after Theorem 1. Figure S3 in the Supplementary Material illustrates that the bands of [Yang and Barber \(2019\)](#) are considerably wider in this application.

Recall that the validity of our bands relies on the isotonicity assumption of p , which we test for as detailed on in Appendix A. The test only rejects isotonicity at the 5% level for the

second model specification displayed on the left side of Figure 5 with a crossing of the lower and upper bounds for probability predictions between 0.1% and 2.7%. Hence, we can directly reject calibration for this model in the critical area of small predictions and furthermore, the remaining calibration band has to be interpreted carefully for this model. As the simulations in Appendix A show that the isotonicity test can even detect slight violations of isotonicity with high power for much smaller sizes as considered in this application, type II test errors are barely a problem here and we can be confident about the isotonicity assumption for the other two model specifications.

For the first model, the calibration band encompasses the diagonal line for all forecast values, meaning that we cannot reject the null hypothesis of perfect calibration $p(x) = x$ at the 5% level. More importantly, we are 95% certain that the true calibration curve lies within the band at any point $x \in [0, 1]$, implying that we are confident that the model is at least as well calibrated as specified by the band. This is especially notable in the important region of predictions below 10% in the magnified right panel of Figure 1, where the calibration bands are remarkably close to the diagonal implying a particularly well calibrated model. E.g., we can conclude that for a prediction of $x = 5\%$, a low birth weight occurs with a probability between 4.6% and 6.7%.

In contrast, we reject calibration for both, the second and third model specifications as shown in Figure 5. However, these bands are much more informative than a simple test rejection as they directly show the exact form of model miscalibration. For the second model specification, we can conclude that the predicted probabilities are particularly miscalibrated for the non-isotonic region discussed above and for values larger than 20%. The third specification entails miscalibrated probabilities for predictions below 10% that are presumably of the highest importance for medical decision making. Finally notice that the wide bands for the third model specification between predicted probabilities of 5% and 20% are caused by little predictions in this interval.

Acknowledgement

T. Dimitriadis gratefully acknowledges financial support from the German Research Foundation (DFG) through grant number 502572912. A. Henzi and J. Ziegel gratefully acknowledge financial support from the Swiss National Science Foundation.

Supplementary material

The Supplementary Material further illustrates the rounding method in simulations, gives details on the low birth weight application and contains additional proofs.

A Detecting and quantifying non-isotonicity

The regression function p could violate isotonicity in (1). Then, its non-isotonicity can be quantified by

$$\gamma(p) := \sup_{x \leq y} \{p(x) - p(y)\} \geq 0.$$

The derivation of our confidence band $(L^{\alpha, \text{raw}}, U^{\alpha, \text{raw}})$ can be adapted as follows: For any index pair $(j, k) \in \mathcal{J}$ and $\delta \in (0, 1)$, we know that

$$\mathbb{P}[\min\{p_j, \dots, p_k\} \leq u^\delta(Z_{jk}, n_{jk})] \geq 1 - \delta, \quad \mathbb{P}[\max\{p_j, \dots, p_k\} \geq \ell^\delta(Z_{jk}, n_{jk})] \geq 1 - \delta. \quad (\text{A1})$$

But the definition of $\gamma(p)$ implies that

$$p(x) \leq \min\{p_j, \dots, p_k\} + \gamma(p) \quad \forall x \leq x_j, \quad p(x) \geq \max\{p_j, \dots, p_k\} - \gamma(p) \quad \forall x \geq x_k.$$

Consequently, one can complement Theorem 1 with the following result:

Table 1: Rejection rates of the isotonicity test

s	Sample size n						
	512	1024	2048	4096	8192	16384	32768
0.5	0.00	0.00	0.00	0.00	0.00	0.00	0.00
0.6	0.00	0.00	0.00	0.00	0.00	0.00	0.00
0.7	0.00	0.00	0.00	0.00	0.01	0.16	0.89
0.8	0.00	0.00	0.01	0.08	0.71	1.00	1.00
0.9	0.00	0.01	0.13	0.85	1.00	1.00	1.00
1.0	0.01	0.14	0.81	1.00	1.00	1.00	1.00

Theorem A1. Let $(L^{\alpha,\text{raw}}, U^{\alpha,\text{raw}})$ be defined as in Theorem 1. Then for any regression function p ,

$$\mathbb{P}\{L^{\alpha,\text{raw}} - \gamma(p) \leq p \leq U^{\alpha,\text{raw}} + \gamma(p)\} \geq 1 - \alpha.$$

This result has two implications: First, a p-value for the null hypothesis that p is isotonic is given by the supremum of all $\alpha \in (0, 1)$ such that $L^{\alpha,\text{raw}} \leq U^{\alpha,\text{raw}}$ pointwise. Second, for a fixed $\alpha \in (0, 1)$ let $\hat{\gamma}_\alpha \geq 0$ be the infimum of all numbers $\gamma \geq 0$ such that $L^{\alpha,\text{raw}} - \gamma \leq U^{\alpha,\text{raw}} + \gamma$. In other words, $\hat{\gamma}_\alpha$ equals $\sup_{x \in \mathbb{R}} \{L^{\alpha,\text{raw}}(x) - U^{\alpha,\text{raw}}(x)\}^+ / 2$. Then $\hat{\gamma}_\alpha$ is a lower $(1 - \alpha)$ -confidence bound for $\gamma(p)$.

Table 1 illustrates the isotonicity test's performance using the Wave specification of Section 5 for $s \geq 0.5$, where $s = 0.5$ entails an isotonic function p , and the choices $s > 0.5$ imply increasing degrees of non-isotonicity, also see Figure 2. We find a conservative test size of zero for $s = 0.5$ and increasing power with both, s and n . For the largest sample sizes, we can detect mild misspecifications with high power, showing that type II errors are barely a concern for the sample size considered in our application.

B Proofs and Technical Lemmas

Lemma B1. Let Y_1, \dots, Y_m be independent Bernoulli variables with expectations $p_1 \leq \dots \leq p_m$, and let $Z = Y_1 + \dots + Y_m$. Then for any $\delta \in (0, 1)$,

$$\Pr\{p_1 \leq u^\delta(Z, m)\} \geq 1 - \delta \quad \text{and} \quad \Pr\{p_m \geq \ell^\delta(Z, m)\} \geq 1 - \delta.$$

Proof of Lemma B1. For the upper bound, note that $u^\delta(z, m)$ is increasing in z . If $b = \min\{z \in \{0, \dots, m\} : u^\delta(z, m) \geq p_1\}$, then $\Pr\{p_1 \leq u^\delta(Z, m)\} = \Pr\{Z \geq b\}$. By Shaked and Shanthikumar (2007, Example 1.A.25), Z is stochastically larger than \tilde{Z} with binomial distribution with parameters m and p_1 , so $\Pr\{Z \geq b\} \geq \Pr\{\tilde{Z} \geq b\} \geq 1 - \delta$, where the last inequality follows from the validity of the Clopper-Pearson confidence bounds. The proof for the lower bound is similar. \square

The proof of Theorem 2 uses standard results for isotonic least squares regression and the following inequalities of Hoeffding (1963, Theorem 1).

Lemma B2. Let Y_1, Y_2, \dots, Y_m be independent random variables with values in $[0, 1]$ and expectations p_1, p_2, \dots, p_m . Suppose that $q = m^{-1} \sum_{i=1}^m p_i \in (0, 1)$, and set $\hat{q} = m^{-1} \sum_{i=1}^m Y_i$. Then for arbitrary $r \in [0, 1]$,

$$\begin{aligned} \Pr(\hat{q} \leq r) &\leq \exp\{-mK(r, q)\} \leq \exp\{-2m(r - q)^2\} \quad \text{if } r \leq q, \\ \Pr(\hat{q} \geq r) &\leq \exp\{-mK(r, q)\} \leq \exp\{-2m(r - q)^2\} \quad \text{if } r \geq q, \end{aligned}$$

where $K(r, q) := r \log(r/q) + (1 - r) \log[(1 - r)/(1 - q)]$.

Corollary B1. For integers $m \geq 1$, $z \in \{0, 1, \dots, m\}$ and any number $\delta \in (0, 1)$,

$$u^\delta(z, m) \leq \max\{\xi \in [\hat{q}, 1] : K(\hat{q}, \xi) \leq \log(1/\delta)/m\} \leq \hat{q} + \sqrt{\log(1/\delta)/(2m)},$$

$$\ell^\delta(z, m) \geq \min\{\xi \in [0, \hat{q}] : K(\hat{q}, \xi) \leq \log(1/\delta)/m\} \geq \hat{q} - \sqrt{\log(1/\delta)/(2m)},$$

where $\hat{q} = z/m$.

In addition, the proof of Theorem 2 makes use of the following proposition which is of independent interest, since it implies a more efficient method for computing the bounds of Yang and Barber (2019).

Proposition B1. For an arbitrary observation vector $\mathcal{Y} \in \mathbb{R}^n$, let $\hat{p}: [0, 1] \rightarrow \mathbb{R}$ be an increasing function minimizing $\sum_{i=1}^n \{Y_i - \hat{p}(x_i)\}^2$. For some $\tau > 0$ and any index $i = 1, \dots, n$, let

$$U_i = \min_{(j,k) \in \mathcal{J}: x_j \geq x_i} \left(\frac{Z_{jk}^{\text{iso}}}{n_{jk}} + \frac{\tau}{\sqrt{n_{jk}}} \right), \quad L_i = \max_{(j,k) \in \mathcal{J}: x_k \leq x_i} \left(\frac{Z_{jk}^{\text{iso}}}{n_{jk}} - \frac{\tau}{\sqrt{n_{jk}}} \right).$$

Then, the minimum for U_i is attained at some $(j, k) \in \mathcal{J}$ such that $j = \min\{s : x_s \geq x_i\}$ and $\hat{p}(x_k) < \hat{p}(x_{k+1})$ or $k = n$. The maximum for L_i is attained at some $(j, k) \in \mathcal{J}$ such that $\hat{p}(x_{j-1}) < \hat{p}(x_j)$ or $j = 1$ and $k = \max\{s : x_s \leq x_i\}$.

Proof of Proposition B1. Consider the statement about U_i . The claim about j follows from the fact that for fixed k , $Z_{jk}^{\text{iso}}/n_{jk}$ is increasing and $n_{jk} = n - j + k$ is decreasing in $j \leq k$. As to the upper index k , note that U_i is the minimum of $u_{jk} = Z_{jk}^{\text{iso}}/n_{jk} + \tau/n_{jk}^{1/2}$ over all $k \geq j = \min\{s : x_s \geq x_i\}$ such that $(j, k) \in \mathcal{J}$. Let $j \leq k_1 < k_2$ be indices such that $\hat{p}(x_k) = \hat{q}$ for $k = k_1 + 1, \dots, k_2$. Then, for $k = k_1, \dots, k_2$,

$$Z_{jk}^{\text{iso}} = Z_{jk_1}^{\text{iso}} + (k - k_1)\hat{q} = B + n_{jk}\hat{q}$$

with

$$B = Z_{jk_1}^{\text{iso}} - n_{jk_1}\hat{q} \begin{cases} \leq 0, \\ = 0 & \text{if } \hat{p}(x_j) = \hat{q}. \end{cases}$$

Consequently, for $k = k_1, \dots, k_2$,

$$u_{jk} = \hat{q} + B/n_{jk} + \tau/n_{jk}^{1/2}$$

is a concave function of $n_{jk}^{-1} \in [n_{jk_2}^{-1}, n_{jk_1}^{-1}]$, and it is increasing in n_{jk}^{-1} if $\hat{q} = \hat{p}(x_j)$. This implies that

$$u_{jk} \geq \begin{cases} \min(u_{jk_1}, u_{jk_2}), \\ u_{jk_2} & \text{if } \hat{q} = \hat{p}(x_j). \end{cases}$$

Consequently, the minimum of u_{jk} over all $k \geq j$ is attained at some $k \geq j$ such that $\hat{p}(x_k) < \hat{p}(x_{k+1})$ or $k = n$, and this entails that $(j, k) \in \mathcal{J}$. The statement about L_i follows from the one about U_i when x_1, \dots, x_n are replaced by $1 - x_n, \dots, 1 - x_1$ and Y_1, \dots, Y_n by $-Y_n, \dots, -Y_1$. \square

Proof of Theorem 2. Define $L_i^{\alpha, \text{YB}} = L^{\alpha, \text{YB}}(x_i)$, $U_i^{\alpha, \text{YB}} = U^{\alpha, \text{YB}}(x_i)$. The inequalities $L_i^{\alpha, \text{nc}} \leq L_i^{\alpha, \text{raw}}$ and $U_i^{\alpha, \text{raw}} \leq U_i^{\alpha, \text{nc}}$, as well as $L_i^{\alpha, \text{YB}} \leq \hat{p}(x_i) \leq U_i^{\alpha, \text{YB}}$ hold by construction. It is therefore sufficient to show that $L_i^{\alpha, \text{YB}} \leq L_i^{\alpha, \text{raw}}$ and $U_i^{\alpha, \text{raw}} \leq U_i^{\alpha, \text{YB}}$. As to the inequality $U_i^{\alpha, \text{raw}} \leq U_i^{\alpha, \text{YB}}$, we know that $U_i^{\alpha, \text{YB}}$ equals

$$u_{jk}^{\text{YB}} = Z_{jk}^{\text{iso}}/n_{jk} + \tau/n_{jk}^{1/2}$$

for some $(j, k) \in \mathcal{J}$ with $j = \min\{s : x_s \geq x_i\}$ and $\hat{p}(x_k) < \hat{p}(x_{k+1})$ or $k = n$, where $\tau = \sqrt{\log\{(N^2 + N)/\alpha\}/2}$. As explained later, this implies that

$$Z_{jk} \leq Z_{jk}^{\text{iso}} \quad \text{if } \hat{p}(x_k) < \hat{p}(x_{k+1}) \text{ or } k = n. \quad (\text{B1})$$

But then it follows from Corollary B1 that $U_i^{\alpha, YB} = u_{jk}^{YB}$ is greater than or equal to

$$Z_{jk}n_{jk}^{-1} + \tau n_{jk}^{-1/2} \geq u^{\alpha/(N^2+N)}(Z_{jk}, n_{jk}) \geq U_i^{\alpha, \text{raw}}.$$

Inequality (B1) follows from a standard result about isotonic regression (see for example Henzi et al., 2022, Characterization II). The index interval $\{j, \dots, k\}$ may be partitioned into index intervals $\{\ell, \dots, m\} = \{j, \dots, n\} \cap \{s : \hat{p}(x_s) = \hat{q}\}$, where \hat{q} is any value in $\{\hat{p}(x_j), \dots, \hat{p}(x_k)\}$. For such an index interval, $Z_{\ell m} \leq Z_{\ell m}^{\text{iso}}$, with equality if $\hat{q} > \hat{p}(x_j)$.

The inequality for the lower bound follows from the one for the upper bound when x_1, \dots, x_n are replaced by $-x_n, \dots, -x_1$ and Y_1, \dots, Y_n by $1 - Y_n, \dots, 1 - Y_1$. \square

References

- Allison, P. J. (2014). Measures of fit for logistic regression. *Paper 1485-2014, SAS Global Forum 2014*, pages 1–12.
- Bertolini, G., D’Amico, R., Nardi, D., Tinazzi, A., and Apolone, G. (2000). One model, several results: the paradox of the Hosmer-Lemeshow goodness-of-fit test for the logistic regression model. *Journal of epidemiology and biostatistics*, 5:251–253.
- Clopper, C. J. and Pearson, E. S. (1934). The use of confidence or fiducial limits illustrated in the case of the binomial. *Biometrika*, 26:404–413.
- Dimitriadis, T., Gneiting, T., and Jordan, A. I. (2021). Stable reliability diagrams for probabilistic classifiers. *Proceedings of the National Academy of Sciences*, 118:e2016191118.
- Dümbgen, L. (1998). New goodness-of-fit tests and their application to nonparametric confidence sets. *The Annals of Statistics*, 26:288–314.
- Guntuboyina, A. and Sen, B. (2018). Nonparametric shape-restricted regression. *Statistical Science*, 33(4):568–594.
- Hall, P. and Horowitz, J. (2013). A simple bootstrap method for constructing nonparametric confidence bands for functions. *The Annals of Statistics*, 41:1892–1921.
- Henzi, A., Moesching, A., and Dümbgen, L. (2022+). Accelerating the pool-adjacent-violators algorithm for isotonic distributional regression. *Methodology and Computing in Applied Probability*. to appear.
- Hoeffding, W. (1963). Probability inequalities for sums of bounded random variables. *Journal of the American Statistical Association*, 58:13–30.
- Hosmer, D. W. and Lemeshow, S. (1980). Goodness of fit tests for the multiple logistic regression model. *Communications in Statistics - Theory and Methods*, 9:1043–1069.
- Hosmer, D. W., Lemeshow, S., and Sturdivant, R. X. (2013). *Applied logistic regression*. Wiley Series in Probability and Statistics. Wiley, Hoboken, N.J, third edition.
- Johnson, N. L., Kemp, A. W., and Kotz, S. (2005). *Univariate discrete distributions*. Wiley Series in Probability and Statistics. Wiley, Hoboken, NJ, third edition.
- Koenker, R. and Yoon, J. (2009). Parametric links for binary choice models: A Fisherian–Bayesian colloquy. *Journal of Econometrics*, 152:120–130.
- Kramer, A. A. and Zimmerman, J. E. (2007). Assessing the calibration of mortality benchmarks in critical care: The hosmer-lemeshow test revisited. *Critical care medicine*, 35:2052–2056.
- Mösching, A. and Dümbgen, L. (2020). Monotone least squares and isotonic quantiles. *Electronic Journal of Statistics*, 14:24–49.
- National Center for Health Statistics (2017). NCHS’ Vital Statistics Natality Birth Data. <https://data.nber.org/data/natality.html>. Online; accessed 13 January 2021.

- Nattino, G., Finazzi, S., and Bertolini, G. (2014). A new calibration test and a reappraisal of the calibration belt for the assessment of prediction models based on dichotomous outcomes. *Statistics in Medicine*, 33:2390–2407.
- Nattino, G., Pennell, M. L., and Lemeshow, S. (2020a). Assessing the goodness of fit of logistic regression models in large samples: A modification of the hosmer-lemeshow test. *Biometrics*, 76:549–560.
- Nattino, G., Pennell, M. L., and Lemeshow, S. (2020b). Rejoinder to “assessing the goodness of fit of logistic regression models in large samples: A modification of the hosmer-lemeshow test”. *Biometrics*, 76:575–577.
- Paul, P., Pennell, M. L., and Lemeshow, S. (2013). Standardizing the power of the Hosmer–Lemeshow goodness of fit test in large data sets. *Statistics in Medicine*, 32:67–80.
- Quinn, J.-A., Munoz, F. M., Gonik, B., Frau, L., Cutland, C., Mallett-Moore, T., Kissou, A., Wittke, F., Das, M., Nunes, T., Pye, S., Watson, W., Ramos, A.-M. A., Cordero, J. F., Huang, W.-T., Kochhar, S., Buttery, J., and Brighton Collaboration Preterm Birth Working Group (2016). Preterm birth: Case definition & guidelines for data collection, analysis, and presentation of immunisation safety data. *Vaccine*, 34(49):6047–6056.
- R Core Team (2022). *R: A language and environment for statistical computing*. R Foundation for Statistical Computing, Vienna, Austria.
- Roelofs, R., Cain, N., Shlens, J., and Mozer, M. C. (2020). Mitigating bias in calibration error estimation. *Preprint*. <https://arxiv.org/abs/2012.08668>.
- Sen, B., Banerjee, M., and Woodroffe, M. (2010). Inconsistency of bootstrap: The Grenander estimator. *The Annals of Statistics*, 38(4):1953–1977.
- Shaked, M. and Shanthikumar, J. G. (2007). *Stochastic orders*. Springer Series in Statistics. Springer, New York.
- Stodden, V., McNutt, M., Bailey, D. H., Deelman, E., Gil, Y., Hanson, B., Heroux, M. A., Ioannidis, J. P., and Taufer, M. (2016). Enhancing reproducibility for computational methods. *Science*, 354(6317):1240–1241.
- Tutz, G. (2011). *Regression for Categorical Data*. Cambridge University Press, Cambridge.
- World Health Organization (2015). *International statistical classification of diseases and related health problems*. World Health Organization. 10th revision, fifth edition. <https://apps.who.int/iris/handle/10665/246208>. Online; accessed 13 January 2021.
- Wright, F. T. (1981). The asymptotic behavior of monotone regression estimates. *Annals of Statistics*, 9:443–448.
- Yang, F. and Barber, R. F. (2019). Contraction and uniform convergence of isotonic regression. *Electronic Journal of Statistics*, 13:646–677.
- Yu, B. and Kumbier, K. (2020). Veridical data science. *Proceedings of the National Academy of Sciences*, 117(8):3920–3929.

Honest calibration assessment for binary outcome predictions

Timo Dimitriadis, Lutz Dümbgen, Alexander Henzi, Marius Puke and Johanna Ziegel

November 4, 2022

The Supplementary Materials contains four parts. Section S.1 demonstrates the effect of using a restricted set of index intervals. Section S.2 gives details on the regression model specifications in the low birth weight application. Section S.3 illustrates the gains of our method upon the wider bands of Yang and Barber (2019) in this application. Section S.4 gives additional proofs.

S.1 The effect of using a restricted family of index intervals

As discussed before equation (7) in the main manuscript and informally described as the rounding method, the confidence bands in equations (4) and (5) also achieve correct coverage in the sense of (2) if we only consider a restricted family of index pairs $\tilde{\mathcal{J}} \subset \mathcal{J}$. Besides the reduced computation time, which we discuss below, this has the additional advantage that it reduces the correction factor of the significance level from $|\mathcal{J}| = N^2 + N$ to $|\tilde{\mathcal{J}}|$. However, the optimal index interval as selected by the infimum in (4) and the supremum in (5) over the full set \mathcal{J} may not be contained in $\tilde{\mathcal{J}}$, resulting in a possibly wider confidence band. While a general balancing of these two opposing effects is difficult without knowledge of the true form of p , Figure S1 illustrates the effect of the rounding method with the explicit choice of $\tilde{\mathcal{J}}$ in (7) based the choices $K \in \{20, 100, \infty\}$ on simulated data.

First assume that the curve p is (almost) flat. Then, the infimum in the computation of $U^{\alpha, \text{raw}}(x)$ in equation (4) is most likely attained for the largest index interval in \mathcal{J} , i.e., by computing the Clopper-Pearson confidence bounds using all indices $x_j \geq x$. Hence, as long as $\tilde{\mathcal{J}}$ in equation (7) approximately contains this full index interval, there is almost no effect of the rounding in terms of an inefficient selection of the index intervals. However, as the correction factor of the significance level is reduced from $N^2 + N$ to $|\tilde{\mathcal{J}}|$, this entails thinner intervals as can be seen in the region $x \geq 0.3$ in Figure S1.

In contrast, in steeper regions of p , the inefficient index interval selection mechanism stemming from a restricted $\tilde{\mathcal{J}}$ might have a bigger adverse effect than the lower correction factor of the significance level. This effect can be observed in the particularly steep region around $x = 0.25$ in the zoomed version of the plot in the right side of Figure S1, where the choice $K = \infty$ yields the most narrow bands. Finally, the region with $x \leq 0.25$ having unit slope (pertaining to the most important case of perfectly calibrated predictions in applications on calibration assessment) shows that rounding with $K = 100$ improves the bands whereas further reducing K results in too coarse approximations, also limiting the adaptivity of the band derived in Theorem 3.

Furthermore, the choice of K in $\tilde{\mathcal{J}}$ massively affects the computation times required for the bands. Figure S2 displays the required computation time to compute the infimum and supremum in equations (4) and (5) for the full index set \mathcal{J} , and two reduced sets $\tilde{\mathcal{J}}$ with $K = 100$ and $K = 1000$ together with the computation time of the Yang and Barber (2019) bands.

As expected, we find that the computation time of our standard method grows at rate n^2 , where computing the bands takes up to 15 minutes for $n = 16\,384$. The computation time decreases drastically for both rounding methods, and even for $K = 1000$, the bands for $n = 16\,384$ are computed within five seconds. For an increasing sample size, the computation time stabilizes once the size of $\tilde{\mathcal{J}}$ stays constant. Finally, the bands of Yang and Barber (2019) have the lowest computation time throughout all considered sample sizes as it suffices to take the minimum over endpoints of constancy regions of the isotonic regression estimate for these bands, which is explained in the end of Section 3 of the main manuscript. The display of the average width on the right-hand side of Figure S2 confirms that medium values of e.g., $K = 100$ or $K = 1000$ yield relatively narrow bands.

Summarizing the results of this section, the rounding method can drastically decrease the computation time and even results in narrower bands for all but very steep regions of the regression function.

S.2 Model specifications in the low birth weight application

We give some additional details on the model specifications of the application here. The first two models are based on the probit link function whereas the third one uses the cauchit link function (Koenker and

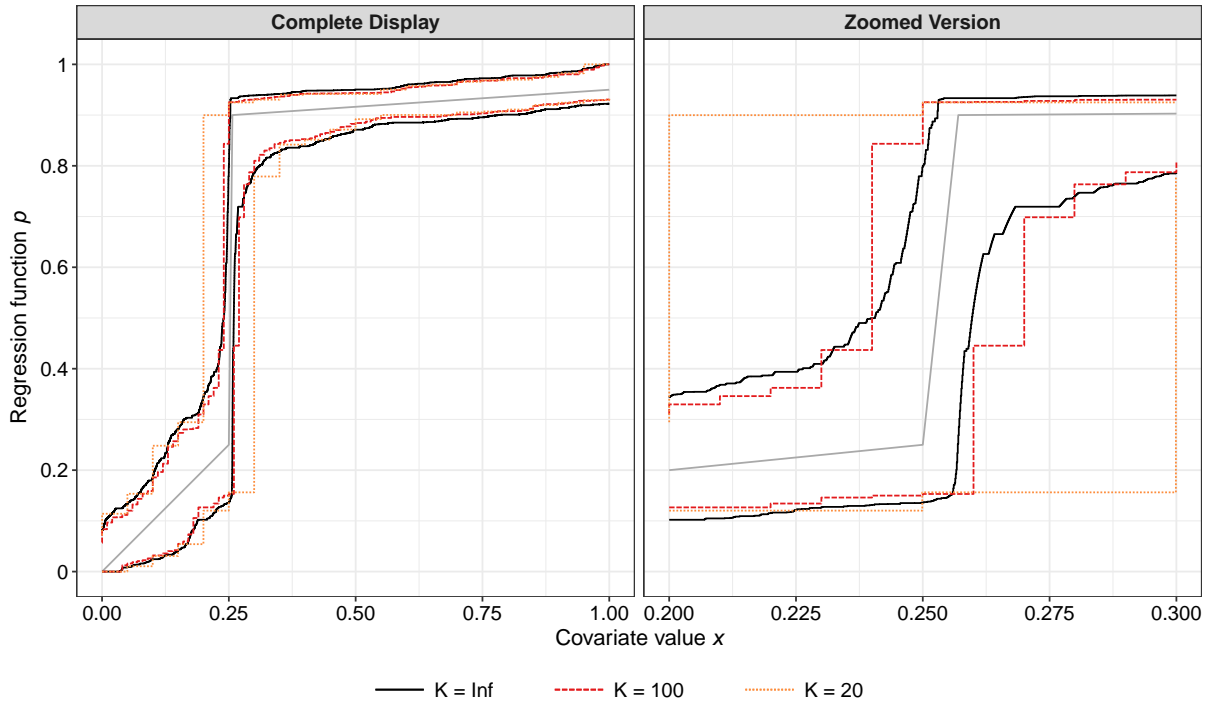


Figure S1: This figure illustrates the effect of the rounding method in (7) with the choices $K \in \{20, 100, \infty\}$, the latter corresponding to no rounding. We simulate $n = 10\,000$ data points with a true regression function $p(\cdot)$ that linearly connects the points $(0, 0)$, $(0.25, 0.25)$, $(0.275, 0.9)$ and $(1, 0.95)$. The left plot shows the true regression function in gray together with the confidence bands and the plot on the right side is a magnified version focusing on the steep area of the regression function.

Yoon, 2009). The second model uses the week of gestation as a continuous variable whereas the first and third models use the week of gestation as a categorical variable with left-closed and right-open intervals with lower interval limits of 0, 28, 32 and 37 weeks, which corresponds to the standard categorization of the World Health Organization (Quinn et al., 2016).

Additionally, all three models contain the following common explanatory variables: the mother’s age and its squared term, her body mass index prior to pregnancy, her smoking behavior as a categorical variable with left-closed and right-open intervals with lower limits of 0, 1, 9, and 20 cigarettes per day averaged over all three trimesters, individual binary variables for mother’s diabetes, any form of hypertension, mother’s education below or equal to eight years, employed infertility treatments, a cesarean in a previous pregnancy, a preterm birth in a previous pregnancy, current multiple pregnancy, the sex of the unborn child, and an infection of one of the following: gonorrhea, syphilis, chlamydia, hepatitis b, hepatitis c. Additional details on the data are given in the user guide under <https://data.nber.org/nativity/2017/natl2017.pdf>.

S.3 The Yang and Barber bands in the low birth weight application

Figure S3 illustrates the bands of Yang and Barber (2019) with a minimal variance factor of $\sigma^2 = 1/4$ in the three binary regression specifications presented in Figures 1 and 5 of the main manuscript. We see that these bands are substantially wider than ours, especially in the most important region of small probability predictions, e.g., illustrated in the zoomed version in the upper right panel of the figure. This improvement is theoretically explained by Theorem 3 (iv) and the corresponding discussion thereafter: Our confidence bands adapt to the variance of the observation, i.e., their width is smaller for p close to zero or one as compared to p around 0.5.

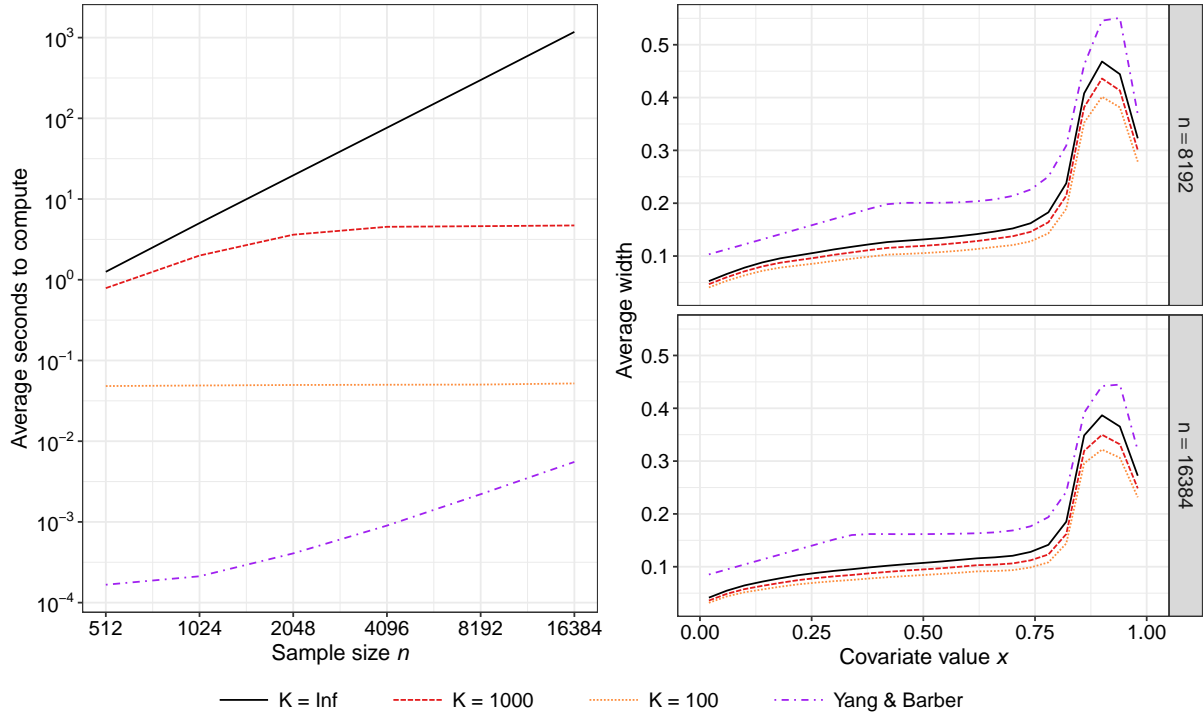


Figure S2: The left plot shows the computation time in simulations of the Kink process with $s = 0.8$ from Section 5 of the main manuscript depending on the sample size for a range of rounding values K and the bands of Yang and Barber (2019). We use a logarithmic scale for both axes. The two plots on the right show the average width of these four versions of the confidence bands depending on the covariate value x .

S.4 Additional Proofs

Proof of Lemma 1. Let $\hat{q}_1 < \dots < \hat{q}_b$ be the different elements of $\{\hat{p}(x_i) : 1 \leq i \leq n\}$, where we assume that $b \geq 2$. There exists a partition of $\{1, \dots, n\}$ into index intervals I_1, \dots, I_b such that $\hat{q}_\ell = |I_\ell|^{-1} \sum_{i \in I_\ell} Y_i$. For any integer $d \geq 1$, let M_d be the number of indices ℓ such that $|I_\ell| = d$. Since $\sum_{i \in I_\ell} Y_i \in \{0, 1, \dots, d\}$, the numbers M_d satisfy the following constraints: $M_d \in [0, d + 1]$, and $\sum_{d=1}^n M_d d = n$. The question is, how large the number $b = \sum_{d=1}^n M_d$ can be under these constraints, where we drop the restriction that the M_d are integers. Suppose that $M_c < c + 1$ and $M_{c'} > 0$ for integers $1 \leq c < c'$. Then we may replace $(M_c, M_{c'})$ with $(M_c + \gamma/c, M_{c'} - \gamma/c')$, where γ is the minimum of $(c + 1 - M_c)c$ and $M_{c'}c'$. This does not affect the constraints, but the sum $\sum_{d=1}^n M_d$ increases strictly, while $M_c = c + 1$ or $M_{c'} = 0$. Eventually, we obtain an integer $d_o \geq 1$ such that $M_d = d + 1$ if $1 \leq d \leq d_o$ and $M_d = 0$ for $d \geq d_o + 2$. In particular,

$$n \geq \sum_{d=1}^{d_o} (d + 1)d = \frac{(d_o + 2)(d_o + 1)d_o}{3} > \frac{d_o^3}{3},$$

whence $d_o < (3n)^{1/3}$, while

$$b \leq \sum_{d=1}^{d_o+1} (d + 1) = \frac{d_o(d_o + 3)}{2} \leq Cn^{2/3},$$

where $C = 3^{2/3}(1 + 3/6^{1/3})/2 < 3$. □

For the proof of Theorem 3, we need an inequality for the auxiliary function $K(\cdot, \cdot)$ in Lemma B2 which follows from Dümbgen (1998, Proposition 2.1).

Lemma S1. For arbitrary $q \in [0, 1]$, $\xi \in (0, 1)$ and $\gamma > 0$, the inequality $K(q, \xi) \leq \gamma$ implies that

$$|\xi - q| \leq \sqrt{2\gamma q(1 - q)} + |1 - 2q|\gamma.$$

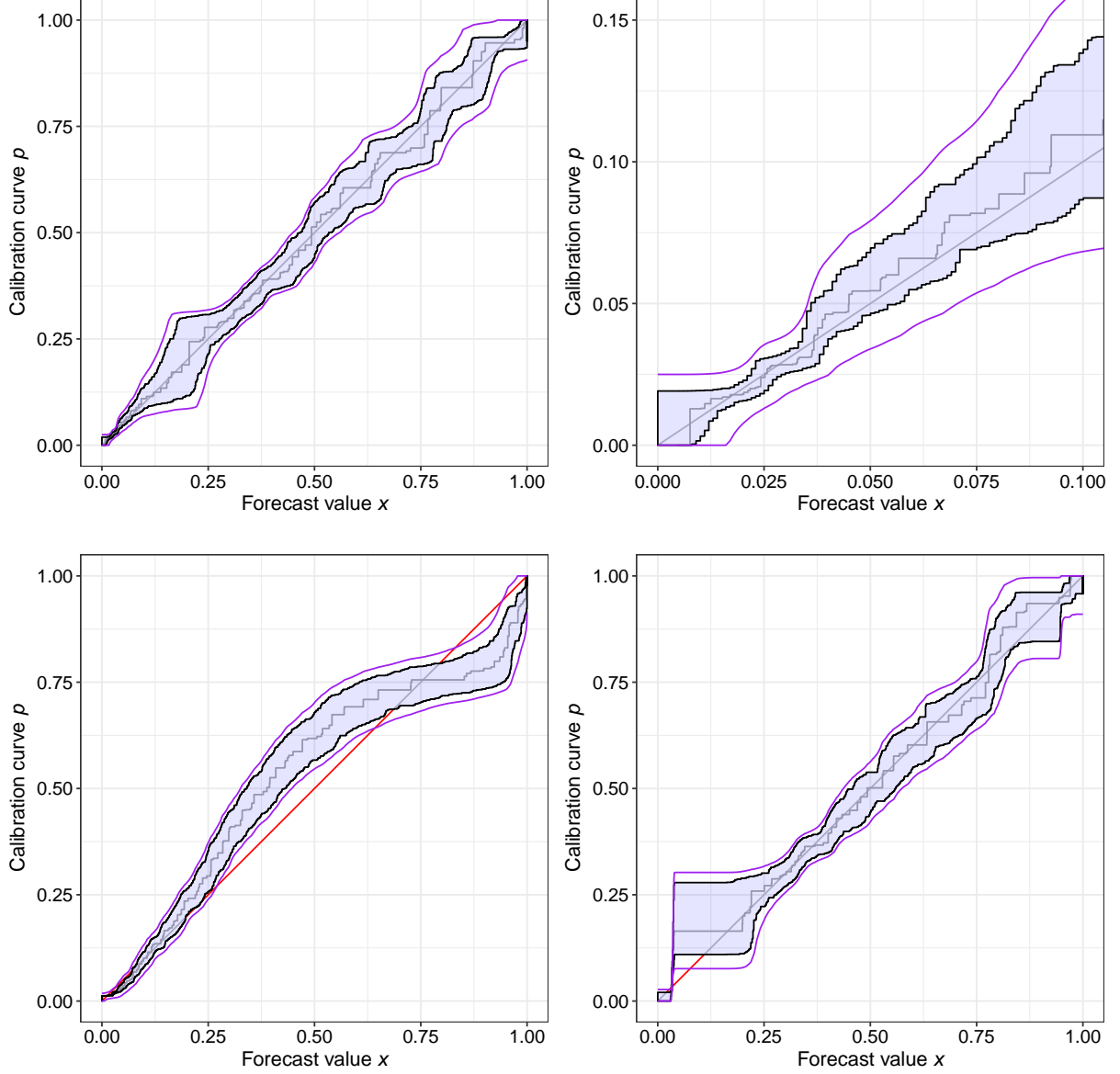


Figure S3: This figures shows the plots given in Figures 1 and 5 augmented with the bands of Yang and Barber (2019) in purple color.

Proof of Theorem 3. For notational convenience, we often drop the additional subscript n , e.g. we write x_i instead of x_{ni} . For symmetry reasons, it suffices to verify the assertions about $U^{\alpha, \text{raw}}$. We only consider sample sizes n such that the inequalities for $W_n(B)$ in Assumption 1 are valid.

In what follows, let C be a generic (large) constant depending only on C_1, C_2 . Its value may change in each instance. It follows from Corollary B1 and Lemma S1 that for sufficiently large n , simultaneously for all $(j, k) \in \mathcal{J}$,

$$u^{\alpha/(N^2+N)}(Z_{jk}, n_{jk}) \leq \hat{p}_{jk} + C \min \left\{ \sqrt{\frac{\log(n)\hat{p}_{jk}}{n_{jk}}} + \frac{\log(n)}{n_{jk}}, \sqrt{\frac{\log(n)}{n_{jk}}} \right\}, \quad (\text{S1})$$

where $\hat{p}_{jk} = Z_{jk}/n_{jk}$. Note that we got rid of α , because $\log\{(N^2 + N)/\alpha\} \leq \log\{(n^2 + n)/\alpha\} = 2\log(n)(1 + o(1))$ as $n \rightarrow \infty$. Moreover, one can deduce from Lemma B2 that simultaneously for all $(j, k) \in \mathcal{J}$,

$$\hat{p}_{jk} \leq p_{jk} + C \sqrt{\frac{\log(n)}{n_{jk}}} \quad (\text{S2})$$

with asymptotic probability one, where $p_{jk} = \mathbb{E}(\hat{p}_{jk}) = n_{jk}^{-1} \sum_{i=j}^k p_i \in [p_j, p_k]$.

As to part (i), let $x \in [a_o, b_o]$ and $B(x) = [x, b_o]$. If $x \leq b_o - C_2\rho_n$, then it follows from Assumption 1 that $B(x) \cap \{x_1, \dots, x_n\} = \{x_{j(x)}, \dots, x_{k(x)}\}$ with $(j(x), k(x)) \in \mathcal{J}$ such that

$$n_{j(x)k(x)} = W_n\{B(x)\} \geq C_1 n(b_o - x).$$

Consequently, we may deduce from inequalities (S1) and (S2) that with asymptotic probability one, simultaneously for all $x \in [a_o, b_o - C_2\rho_n]$,

$$U_n^{\alpha, \text{raw}}(x) \leq u^{\alpha/(N^2+N)}(Z_{j(x)k(x)}, n_{j(x)k(x)}) \leq \hat{p}_{j(x)k(x)} + C\sqrt{\rho_n/(b_o - x)},$$

$$\hat{p}_{j(x)k(x)} \leq p_{j(x), k(x)} + C\sqrt{\rho_n/(b_o - x)} = p(x) + C\sqrt{\rho_n/(b_o - x)}.$$

These two inequalities imply that $U_n^{\alpha, \text{raw}}(x) \leq p(x) + C\sqrt{\rho_n/(b_o - x)}$ for $x \in [a_o, b_o - C_2\rho_n]$. But for $x \in [b_o - C_2\rho_n, b_o]$, the term $\sqrt{\rho_n/(b_o - x)}$ is at least $C_2^{-1/2}$, and $U_n^{\alpha, \text{raw}}(x) - p(x) \leq 1$. Hence we can deduce part (i) by replacing C with $\max\{C, C_2^{1/2}\}$.

As to part (ii), let $B(x) = [x, x + h_n]$ for $x \in [a_o, b_o - h_n]$ with some constant $h_n \geq C_2\rho_n$ to be determined later. By Assumption 1, $B(x) \cap \{x_1, \dots, x_n\} = \{x_{j(x)}, \dots, x_{k(x)}\}$ with $(j(x), k(x)) \in \mathcal{J}$ satisfying

$$n_{j(x)k(x)} = W_n\{B(x)\} \geq C_1 n h_n.$$

Consequently, we may deduce from inequalities (S1), (S2) and Lipschitz-continuity of p on $[a_o, b_o]$ with Lipschitz constant L that with asymptotic probability one, simultaneously for all $x \in [a_o, b_o - h_n]$,

$$\begin{aligned} U_n^{\alpha, \text{raw}}(x) &\leq u^{\alpha/(N^2+N)}(Z_{j(x)k(x)}, n_{j(x)k(x)}) \leq \hat{p}_{j(x)k(x)} + C\sqrt{\rho_n/h_n}, \\ \hat{p}_{j(x)k(x)} &\leq p_{j(x), k(x)} + C\sqrt{\rho_n/h_n}, \\ p_{j(x)k(x)} &\leq p(x) + Lh_n. \end{aligned}$$

These three inequalities imply that $U_n^{\alpha, \text{raw}}(x) \leq p(x) + C\sqrt{\rho_n/h_n} + Lh_n$. If we set $h_n = \rho_n^{1/3} L^{-2/3}$, the upper bound becomes $C(L\rho_n)^{1/3}$. This requires $\rho_n^{1/3} L^{-2/3} \geq C_2\rho_n$, though. But in case of $\rho_n^{1/3} L^{-2/3} \leq C_2\rho_n$, the term $(L\rho_n)^{1/3}$ is at least $C_2^{-1/2}$, so we can deduce part (ii) by replacing C with $\max\{C, C_2^{1/2}\}$.

Part (iii) can be verified similarly as part (i). let $B(x) = [x, x_o]$ for $x \in [a_o, x_o]$. In case of $x \leq x_o - C_2\rho_n$, $B(x) \cap \{x_1, \dots, x_n\} = \{x_{j(x)}, \dots, x_{k(x)}\}$ with $(j(x), k(x)) \in \mathcal{J}$ such that $n_{j(x)k(x)} \geq C_1 n(x_o - x)$. Thus it follows from inequalities (S1) and (S2) that with asymptotic probability one, simultaneously for all $x \in [a_o, x_o - C_2\rho_n]$,

$$U_n^{\alpha, \text{raw}}(x) \leq u^{\alpha/(N^2+N)}(Z_{j(x)k(x)}, n_{j(x)k(x)}) \leq \hat{p}_{j(x)k(x)} + C\sqrt{\rho_n/(b_o - x)},$$

$$\hat{p}_{j(x)k(x)} \leq p_{j(x), k(x)} + C\sqrt{\rho_n/(b_o - x)} \leq p(x_o -) + C\sqrt{\rho_n/(b_o - x)}.$$

If $x \in [x_o - C_2\rho_n, x_o]$, the term $\sqrt{\rho_n/(b_o - x)}$ is at least $C_2^{-1/2}$, so we can deduce part (iii) by replacing C with $\max\{C, C_2^{1/2}\}$.

To verify part (iv), let $B(x, y) = [x, y]$ for $a_o \leq x < y \leq b_o$. If $y - x \geq C_2\rho_n$, then $B(x, y) \cap \{x_1, \dots, x_n\} = \{x_{j(x,y)}, \dots, x_{k(x,y)}\}$ with $(j(x, y), k(x, y)) \in \mathcal{J}$ such that $n_{j(x,y)k(x,y)} \geq C_1 n(y - x)$. Hence, it follows from (S1) and $p_{j(x,y)k(x,y)} \leq p(y)$ that

$$\begin{aligned} \mathbb{E}\{U_n^{\alpha, \text{raw}}(x_n)\} &\leq \mathbb{E}\{u^{\alpha/(N^2+N)}(Z_{j(x,y)k(x,y)}, n_{j(x,y)k(x,y)})\} \\ &\leq \mathbb{E}\left\{\hat{p}_{j(x,y)k(x,y)} + C\left(\sqrt{\hat{p}_{j(x,y)k(x,y)}\rho_n/(y-x)} + \rho_n/(y-x)\right)\right\} \\ &\leq p_{j(x,y)k(x,y)} + C\left(\sqrt{p_{j(x,y)k(x,y)}\rho_n/(y-x)} + \rho_n/(y-x)\right) \\ &\leq p(y) + C\left(\sqrt{p(y)\rho_n/(y-x)} + \rho_n/(y-x)\right) \\ &\leq C\{p(y) + \rho_n/(y-x)\}, \end{aligned}$$

where the third inequality follows from Jensen's inequality, and the last inequality follows from $\sqrt{st} \leq (s+t)/2$ for $s, t \geq 0$. This is true if $y - x \geq C_2\rho_n$. But in case of $y - x \leq C_2\rho_n$, the term $\rho_n/(y-x)$ is at least C_2^{-1} , so we can deduce part (iv) by replacing C with $\max\{C, C_2\}$. \square